

Point-Focusing Shear-Horizontal Guided Wave EMAT Optimization Method Using Orthogonal Test Theory

Hongyu Sun, Shen Wang, Songling Huang, Senior Member, IEEE, Lisha Peng, Student Member, Qing Wang, Senior Member, IEEE, Wei Zhao and Jun Zhou

Abstract—As a class of devices used in sound detection, electromagnetic acoustic transducers (EMATs) have been widely used in the field of nondestructive testing (NDT) owing to their advantages such as contact-free operation, wide applicability, and high performance. However, their low energy-conversion efficiency is the main drawback that limits usage in industrial testing. In this work, we report the effect of different parameters of the point-focusing shear-horizontal EMAT (PFSH_EMAT) on the signal intensity of the receiving transducer. The impact factors of the focusing transducer are as follows: number of magnets in a row m , fan-shaped periodic permanent magnet (FPPM) remanence magnetization B_r , coil width w , coil winding number n , aperture angle θ , focal length I_f , life-off distance h_1 , excitation current frequency f_c and current amplitude I_c . To improve the analysis efficiency, and L32(4⁹) orthogonal table is used to investigate the nine different factors at four levels, which can be calculated through finite element simulations. The effect of each factor on the signal intensity is obtained by range analysis, and the influence degree of each factor is obtained, and the parameter combination is optimized by analyzing the test results to improve the PFSH-EMAT's performance. The experimental results show that the optimized PFSH-EMAT is 170% more efficient than the average of the top-three signal intensities in the orthogonal test, which proves the effectiveness of the proposed optimization method.

Index Terms—Point-focusing, shear horizontal guided wave, orthogonal test, range analysis, optimization method, signal intensity.

I. INTRODUCTION

NONDESTRUCTIVE testing (NDT) technology has been widely used in industrial online monitoring as a detection method that does not damage a specimen [1]–[6]. There are five primary methods to detect defects: ultrasonic, radiographic, magnetic leakage, penetrant, and eddy current testing [7], [8]. The ultrasonic testing method is widely used in online defect detection in complex environments owing to its higher detection speed and accuracy [9]. The ultrasonic guided wave detection technology using piezoelectric ultrasonic transducers requires coupling the ultrasonic vibration into the specimen using a couplant. Therefore, piezoelectric based transducers are difficult to use in condition that require

noncontact operation and high temperatures [10],[11]. In addition, air-coupled transducers have the advantage of non-contact operation and are independent of the couplant. However, the ultrasonic waves generated by the air coupling method experience severe energy attenuation owing to the excessive gap of the acoustic impedance, especially when the waves pass through the interface between the air and specimen [12], [13].

Electromagnetic acoustic transducers (EMATs) rely on the electromagnetic coupling to achieve energy conversion of the alternating current in the transducer coil to mechanical vibration in the specimen, thus foregoing the requirement of a coupling medium. Ultrasonic guided waves can be directly generated by an EMAT in the specimen and can be used for inspection under special conditions such as noncontact and high-temperature operation [14]. Although EMATs have significant advantages in the detection of defects, their energy conversion efficiency is very low compared to other transducers, including piezoelectric transducers. Therefore, improving the conversion efficiency of an EMAT has garnered much attention, and many methods have been proposed to solve this problem. Increasing the excitation current of the coils is an intuitive and widely used method to improve the signal-to-noise ratio (SNR) of the EMAT [15]. Although this method cannot improve energy conversion efficiency, it enables the convenient extraction of ultrasonic signals. However, to generate a large current, a complicated and expensive device is required, and there may be safety problems in detection. Other methods to improve conversion efficiency include ultrasound arrays and signal processing, but these methods have their limitations for detection.

In recent years, electromagnetic ultrasonic focusing technology has provided an effective alternative to solve the problem of low EMAT conversion efficiency. The sensitivity and signal intensity are two critical factors that affect EMATs focusing capabilities. For body wave focusing, line and point focusing EMATs were proposed and developed, and the impact factors were discussed [16]–[18]. However, the detection accuracy of the ultrasonic body wave is relatively low, so it is difficult to achieve high-speed detection. Therefore, ultrasonic guided waves are generally used to detect defects in large plates or pipes. The shear-horizontal (SH) guided wave is a widely

used wave mode for detecting plate defects because it has particular advantages: zero out-of-plane displacement and no dispersion for SH₀ mode [19], [20]. Therefore, it is necessary to achieve SH guided wave focusing to improve the performance of the EMAT. Song et al. proposed a focusable and rotatable SH guided wave EMAT that could strengthen the wave on the closing side of the line source; they concluded that the unidirectional excitation capability and directionality of the EMAT were significantly improved [21]. However, more than one EMAT was used, which could cause extra reflected and refracted SH guided waves; thus, this method requires a precise mechanical structure for accurate direction adjustment. Moreover, the effects of various parameters on the focusing performance were not studied. According to the propagation theory of SH guided wave and considering phase superposition, the point-focusing SH EMAT (PFSH-EMAT) was proposed by Sun et al., and unidirectional focusing was achieved by double excitation coils with phase difference or oblique focusing fan-shaped periodic permanent magnets (FPPMs) [22]–[24]. The results show that the focusing effect is noticeable, and the signal intensity at the focal point is effectively improved. Although the authors studied the effects of several factors on the focusing capability of the newly designed PFSH-EMAT, the influence degree and optimal combination of impact parameters were not given. There are also multiple optimization methods, and some optimization methods can be applied to different types of models. Methods for solving optimization problems can generally be divided into analytical methods, numerical methods, and other methods. At present, the orthogonal test method is used to study the optimization of EMAT parameters [25], [26]. The orthogonal test has advantages such as high efficiency, timesaving, saving sample content, and the influence degree and trend of various factors can be obtained. Furthermore, genetic algorithms are currently widely used as artificial intelligence optimization algorithms. As a global optimization method, this method can give precise control conditions when the optimal control point is included in the test range. When the optimal control point is not included in the test range, the test range can be expanded. This can be supplemented as an optimization method for orthogonal experiments. However, this genetic algorithm also has its shortcomings, including precocious, more calculations required, the processing scale is small, difficult to deal with nonlinear constraints, and poor stability. Because the algorithm is a random algorithm and needs multiple operations, and the reliability of the result is poor, and the solution cannot be obtained stably. Therefore, considering the functionality, applicability, purpose, and comparative advantages of the algorithm, we choose the orthogonal test method as the research method in the paper.

In this work, we study the effects of different parameters of the PFSH-EMAT on their focusing capability with finite element simulation and experiments using the orthogonal test method. The nine parameters selected are as follows: the number of magnets in a row m , FPPM remanence magnetization B_r , coil width w , coil winding number n , aperture angle θ , focal length l_f , lift-off distance h_l , excitation

current frequency f_c , and current amplitude I_c . In addition, the test result is given as the signal intensity M . The outline of this work is as follows. First, the influence parameters are determined through physical analysis, and a particular combination of parameters is calculated through simulations to extract the required signal intensity. Next, according to the selected parameters and levels, an L32(49) orthogonal table is determined, and the parameter combination in the orthogonal table is calculated by the Finite Element Method (FEM) to obtain the focusing signal intensities under different parameter combinations. Then, through the range analysis of the test results, the effects of different parameters on the signal intensity are obtained, and the relationships between the parameter trends and signal intensities are assessed. Finally, the optimal parameter combination of a PFSH-EMAT based on range analysis results is obtained and verified through experiments.

II. DESIGN OF PFSH-EMATS

A. Theoretical Method

As a device for generating ultrasonic waves, EMAT is mainly based on the theory of Lorentz force, magnetization, and magnetostriction inside the specimen. In the detection of ultrasound on aluminum plates, the influence of Lorentz force dominates, and the magnetization and magnetostriction mechanisms are negligible [14]. Therefore, the process of EMAT generating ultrasonic waves in an aluminum plate can be described as the alternating current coils induce an alternating eddy current on the aluminum plate surface, and the induced current generates a Lorentz force under the effect of an external bias magnetic field. This cyclically varying Lorentz force causes the aluminum plate to vibrate, thereby transmitting sound waves in a particular mode such as SH guided wave, SV body wave, and Rayleigh surface waves [27]–[29]. Therefore, the generation of ultrasonic waves is a multi-physical coupling process, and the Lorentz force is the main factor to connect different physical fields as a coupling variable.

To study the focusing capability of a PFSH-EMAT, it is necessary to analyze its mechanism before further discussion. The excitation process of the SH guided wave includes the coupling of two physical fields: an electromagnetic field and a dynamic elastic field. The electromagnetic field mainly describes the distribution of eddy currents in an aluminum plate, and Maxwell's equations can be used to describe this physical process as [23].

$$\sigma \frac{\partial A}{\partial t} - \frac{1}{\mu} \nabla^2 A = J_s, \quad (1)$$

where A is the magnetic field potential; σ is the conductivity; J_s is the source current density. The eddy current can be expressed as

$$J_e = -\sigma \frac{\partial A}{\partial t}. \quad (2)$$

As mentioned above, the eddy current J_e will generate

Lorentz force F_v in the aluminum plate under the applied bias static magnetic field B_s , and the dynamic magnetic field B_d generated by the dynamic magnetic field potential will also affect the Lorentz force.

$$F_v = J_e \times (B_d + B_s), \quad (3)$$

The dynamically changing eddy current and background magnetic field produce varying Lorentz force F_v , which connects the two physical fields, because the external force causes the aluminum plate to be elastically deformed, thereby generating ultrasonic waves by vibration. This process can be described by the following wave equation.

$$(\kappa + G) \nabla \nabla \cdot \mathbf{u} + G \nabla^2 \mathbf{u} + F_v = \rho \frac{\partial^2 \mathbf{u}}{\partial t^2}, \quad (4)$$

where \mathbf{u} is the displacement vector; t is the time; ρ is the mass density; κ and G are the Lamé's constants of the material, which affects the propagation velocity of the shear and longitudinal waves in an aluminum plate. Eq. (4) shows that the position of the particle in the specimen changes with time and is related to the Lorentz force. Moreover, for the receiving transducer, the process of the ultrasonic signal reception is actually the inverse of the ultrasonic generation, because the structure of the EMAT can both transmit and receive ultrasonic waves [18], [30]. In order to achieve higher intensity signals from the receiving transducers, it is necessary to analyze and study the generation, transmission and reception processes of an EMAT.

focus SH guided waves to a point was proposed [22]. The configuration of this EMAT is shown in Fig. 1(a-c).

As shown in Fig. 1(c), an FPPM is used to generate the bias magnetic field, and the remanence magnetization of the magnets is B_r , the number of magnets in a row is m . The coil with the number of turns n is evenly wound around the FPPM, and the concentric point of the coil is the center of the FPPM, also named as the focal point. For the setting of the coordinate system, the main propagation direction of the SH guided wave is defined as the x -axis, the vibration direction is the y -axis, and the z -axis represents the normal direction of the aluminum plate surface. Other parameters that can be used to describe the characteristics of a PFSH-EMAT are shown in Fig. 1(a,b). The aperture angle θ is defined as the angle between the first and last line sources of the fan-shaped coils. The focal length l_f is the distance between the focal point and the middle of the FPPM. The width of a coil is w and the excitation current on the coil is a burst current with an amplitude I and frequency f_c . Since the size of the permanent magnet has a large influence on the bias magnetic field, so the length l_s of a single magnet is considered, and the lift-off distance h_l is shown in Fig. 1(b).

In the design of a PFSH-EMAT, it is necessary to ensure that the SH guided waves generated by the respective coils can achieve phase superposition. Therefore, to achieve the maximum amplitude of the acoustic wave during the propagation process, the magnet length l_s and the frequency f_c need to satisfy the following matching relationship.

$$l_s = \frac{\lambda}{2} = \frac{c_s}{2f_c}, \quad (5)$$

where λ is the wavelength, and C_s is the velocity of shear waves.

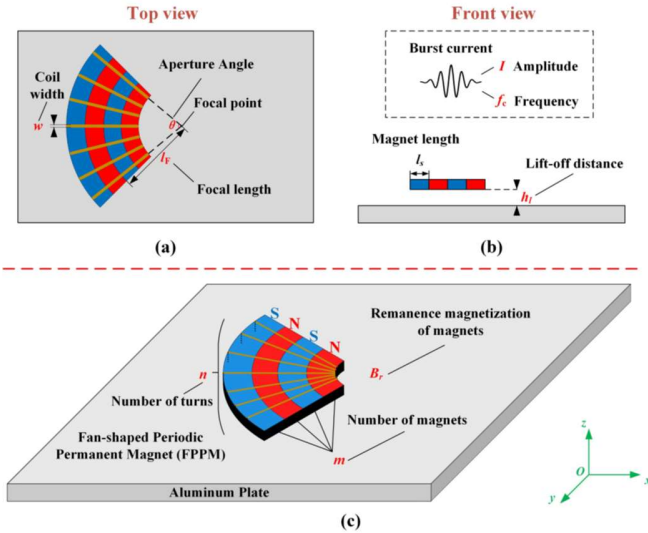


Fig.1 Configuration of PFSH-EMAT: (a) a top view; (b) a front view; (c) 3D setup.

B. Configuration of PFSH-EMATs

In previous studies, a newly designed PFSH-EMAT that can

C. Numerical Algorithm

COMSOL is widely used in scientific research as a multi-physical simulation software. The governing equations describing the physical process of an EMAT can be fully described in this software. Calculation of the Lorentz force is solved by the joint-calculation using the AC/DC Module and the magnetic field (no current) module in the manuscript. Moreover, the solid mechanic module with the linear elastic material is utilized to calculate the propagation process of SH waves. With the coupling of Lorentz force among the various modules, the calculation of each physical field will perform simultaneously and couple to each other. The constant parameters in the simulation are shown in Table I.

TABLE I
PARAMETERS OF THE SEPECIMEN

Parameters	Value
Specimen Lamé's constants k (Gpa)	58
Specimen Lamé's constants G (Gpa)	29
Specimen mass density (kg/m^3)	2832
Specimen conductivity (S/m)	3.65×10^7
Magnet relative permeability	400
Magnet coercive force (MA/m)	0.9

Since the magnitude I and frequency f_c of the excitation current affect the mode and amplitude of the SH guided wave,

it is also important to determine the reasonable excitation current properties in the EMAT's design and optimization. In this work, a burst current is selected as the excitation waveform of the coil, and the current waveform can be expressed as

$$i(t) = I_c e^{-\alpha(t-\tau)^2} \cos[2\pi f_c(t-\tau) + \theta_d], \quad (6)$$

where I_c is the amplitude of the signal, $\alpha = 5 \times 10^{11} \text{s}^{-2}$ is the bandwidth factor, $\tau = 4 \mu\text{s}$ is the arrival time, f_c is the central frequency, and $\theta_d = 0^\circ$ is the phase delay. To improve the computational efficiency and experimental accuracy, it is necessary to design the geometry of the aluminum plate properly to match different aperture angles θ , focal lengths l_f and FPPM dimensions. The thickness of the aluminum plate is specified to be 1.5 mm here.

III. DESIGN AND STUDY OF ORTHOGONAL TEST

A. Background and Parameter Selection

Orthogonal test design refers to a design method that studies multi-factors and multi-levels. Based on the orthogonality, some representative points are selected from the full test, and these representative points were uniformly dispersed and neatly comparable [31]. The orthogonal table is used as the main tool of the orthogonal test, and its selection depends on the number and level of factors in the test, then the representative points are selected from the full test. The method of replacing large-scale tests with very few tests will significantly improve the efficiency of scientific analysis. Therefore, as an efficient multi-factor experimental design method, the orthogonal test method is chosen in this paper to analyze the influence of different transducer parameters on the focusing capability [32]. In the selection of the parameters that affect the PFSH-EMAT's focusing capability, it is necessary to first determine which factors affect the signal received by the receiving transducer. The SNR of the received signal is [33]

$$SNR = \frac{I_c n^2 B_r A}{2 Z_S \sqrt{K T \beta} R_{EMAT}} \exp\left(-\frac{\alpha h_l}{w}\right), \quad (7)$$

where I_c is the excitation current; n is the coil winding number; B_r is the bias magnetic flux density; A is the active area; Z_S is the acoustic dependence; α is a geometry constant; h_l is the lift-off distance; w is the coil width; K is Boltzmann's constant times the electronic charge; T is temperature; β is the amplifier bandwidth and R_{EMAT} is the coil resistance.

It can be obtained from Eq. (7) that the following thirteen parameters will influence the signal amplitude effectively: current with amplitude I_c and frequency f_c ; coil winding number n , width w , length l_c ; FPPM's remanence magnetization B_r , number of magnets in a row m , inner radius r and outer radius R , magnet length l_s ; lift-off distance h_l ; focal distance l_f ; aperture angle θ . However, these parameters are not all independent, some of them have interactions. Eq. (5) shows the relationship between magnet length l_s and current frequency f_c , and focal length $l_f = (R+r)/2$, $(R-r)/l_s = m$. Therefore, nine

representative parameters are selected and the appropriate levels are determined as shown in Table II.

TABLE II
FACTORS AND LEVELS OF ORTHOGONAL TEST

Parameters	Level 1	Level 2	Level 3	Level 4
m	4	6	8	10
Br (T)	0.6	0.8	1	1.2
W (mm)	0.2	0.4	0.6	0.8
n	5	9	13	17
θ ($^\circ$)	20	40	60	80
l _f (mm)	50	100	150	200
h _l (mm)	0.5	1	1.5	2
f _c (kHz)	500	600	700	800
I _c (A)	50	100	150	200

It should be noted that the phase velocity of the SH0 mode wave does not change with the frequency-thickness product, and the SH0 wave mode has no dispersion, so the SH0 mode guided wave has great advantages in detecting defects. Therefore, the following formula needs to be satisfied in selecting the level of factors [23]

$$f d \leq \frac{\beta c_s}{2}, \quad (8)$$

where d is the thickness of the aluminum plate and it is fixed to 1.5 mm in this paper; β should be a positive integer to avoid the presence of any higher-order wave modes. The drive frequency of the current should be less than 1.07 MHz. Then the levels of the current frequency are set from 500-800 kHz.

To determine the level of each factor, in the design of m level, the following measurement problems should be considered: low measurement accuracy, hard in permanent magnet design, limited effective focal length, and higher requirements on the specimen surface. And in terms of processing technology, the diameter of the EMAT probe is generally about 10-30 mm. Therefore, m should be smaller than 10 in our design and testing. In addition, the value range of B_r depends on the high-temperature environment of EMAT. Moreover, the width of the coil w is required to meet the requirement of maximum current I passing. Because the maximum width w of the coil is 0.8 mm, the size of the aperture angle must also be satisfied. Therefore, considering the minimum focal length, it can be obtained from the calculation of the trigonometric function that a reasonable value of n is 17 at most, and exceeding this value will cause the calculation positions of the coils to be overlapped, which cannot be achieved in experiments. The range of aperture angles θ is determined by the vertical component of the guided waves. Then, considering both sensitivity and stability of the transducer, the levels of the lift-off distance h_l are set from 0.5-2 mm. Furthermore, for focal length l_f , within a reasonable range, this value is determined by actual needs.

For all parameters, each factor is set to four levels, then an

L32(4⁹) orthogonal table is selected. Moreover, each orthogonal test needs one or more results that can be analyzed, and the magnitude of the signal intensity is an important reflect of the focusing transducer's performance, so the signal amplitude M is chosen in this paper [34].

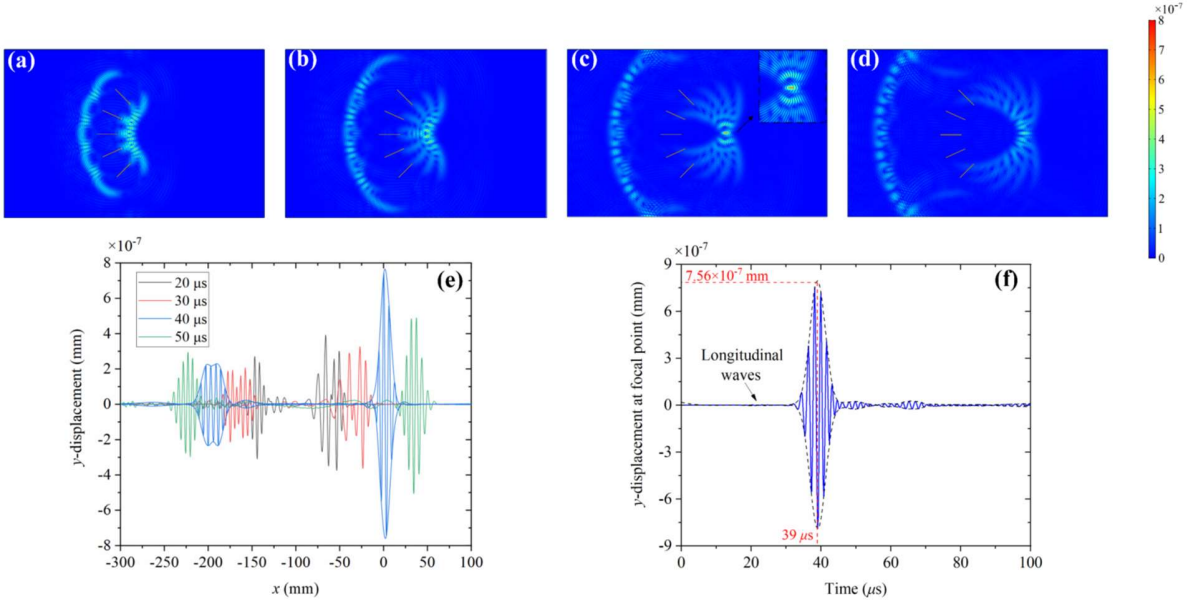


Fig. 2 Simulation results of the PFSH-EMAT when $m=4$, $B_r=0.6$ T, $w=0.8$ mm, $n=1$, $\theta=80^\circ$, $L_f=100$ mm, $h_l=1.5$ mm, $f_c=600$ kHz and $I_c=150$ A: (a) displacement distribution at $20 \mu\text{s}$; (b) displacement distribution at $30 \mu\text{s}$; (c) displacement distribution at $40 \mu\text{s}$; (d) displacement distribution at $50 \mu\text{s}$; (e) displacement distribution along x-axis at different moments; (f) displacement at the focal point.

B Simulation Analysis

After the parameters required by the EMAT are determined, the calculation can be performed by simulation. We use a 3-D simulation model [32], and the dynamic Lorentz force exists only in the plane of the specimen and changes periodically. As a special case, the factors are selected as: $m=4$, $B_r=0.6$ T, $w=0.8$ mm, $n=1$, $\theta=80^\circ$, $L_f=100$ mm, $h_l=1.5$ mm, $f_c=600$ kHz and $I_c=150$ A. Under this condition, the simulation results can be shown in Fig. 2(a-f). To demonstrate the wave propagation process, Figs. 2(a-d) show the displacement distribution on the aluminum plate at different moments of $20 \mu\text{s}$, $30 \mu\text{s}$, $40 \mu\text{s}$, and $50 \mu\text{s}$. The figures show that when the time reaches $40 \mu\text{s}$, the SH wave generated by each coil will reach the focal point at the same moment. From the simulation in Fig. 2(c), the enlarged figure shows that the guided waves are focused at the focal point successfully.

Fig. 2(e) quantitatively describes the displacement field distribution of the aluminum plate surface in Figs. 2(a-d) along the x-axis. It is shown that the signal intensity reaches its peak at $40 \mu\text{s}$, and the waves reach the focal point at this moment and the focal distance is 100 mm, which is the pre-determined factor of the simulation. Therefore, the point focusing capability of a PFSH-EMAT is obvious. Fig. 2(f) shows the displacement at the focal point over time, and longitudinal waves can be observed as its velocity is twice that of shear waves. The wave displacement is 7.56×10^{-7} mm, and the moment is $39 \mu\text{s}$. Based on the simulation method and result mentioned above, the signal intensity M at different factor level combinations can be obtained.

TABLE III
L₃₂ (4⁹) ORTHOGONAL TABLE

No.	Factors									Results	
	A	B	C	D	E	F	G	H	I	M	
	m	B_r	w	n	θ	L_f	h_l	f_c	I_c	($\times 10^{-7}$)	
	l	T	mm	l	$^\circ$	mm	mm	kHz	A		mm
1	4	0.6	0.2	5	20	50	0.5	500	50	10.15	
2	4	0.8	0.4	9	40	100	1	600	100	17.63	
3	4	1	0.6	13	60	150	1.5	700	150	13.54	
4	4	1.2	0.8	17	80	200	2	800	200	5.983	
5	6	0.6	0.2	9	40	150	1.5	800	200	2.333	
6	6	0.8	0.4	5	20	200	2	700	150	1.304	
7	6	1	0.6	17	80	50	0.5	600	100	301.1	
8	6	1.2	0.8	13	60	100	1	500	50	62.54	
9	8	0.6	0.2	13	80	50	1	700	200	61.54	
10	8	0.8	0.4	17	60	100	0.5	800	150	53.25	
11	8	1	0.6	5	40	150	2	500	100	4.631	
12	8	1.2	0.8	9	20	200	1.5	600	50	7.531	
13	10	0.6	0.2	17	60	150	2	600	50	1.971	
14	10	0.8	0.4	13	80	200	1.5	500	100	5.402	
15	10	1	0.6	9	20	50	1	800	150	93.97	
16	10	1.2	0.8	5	40	100	0.5	700	200	135.8	
17	4	0.6	0.2	5	80	100	1.5	600	150	7.562	
18	4	0.8	0.4	9	60	50	2	500	200	13.58	
19	4	1	0.6	13	40	200	0.5	800	50	10.71	
20	4	1.2	0.8	17	20	150	1	700	100	15.87	
21	6	0.6	0.2	9	60	200	0.5	700	100	42.9	
22	6	0.8	0.4	5	80	150	1	800	50	3.208	
23	6	1	0.6	17	20	100	1.5	500	200	52.41	
24	6	1.2	0.8	13	40	50	2	600	150	7.55	
25	8	0.6	0.2	13	20	100	2	800	100	3.28	
26	8	0.8	0.4	17	40	50	1.5	700	50	19.9	
27	8	1	0.6	5	60	200	1	600	200	11.28	
28	8	1.2	0.8	9	80	150	0.5	500	150	139.8	
29	10	0.6	0.2	17	40	200	1	500	150	69.21	
30	10	0.8	0.4	13	20	150	0.5	600	200	354.6	
31	10	1	0.6	9	80	100	2	700	50	0.8132	
32	10	1.2	0.8	5	60	50	1.5	800	100	14.41	

C Results and Discussions of Orthogonal Array Test

As described above, factors and levels of the PFSH-EMAT are determined using an L₃₂(4⁹) orthogonal table, and the simulation result using these parameters will give the signal intensity M as the test result. The orthogonal table including nine factors and four levels is shown in Table III.

By analyzing the results of these 32 orthogonal tests, it is

possible to replace all of the 262 144 full tests. To evaluate the influence degree of the nine factors on test results, the range analysis of the orthogonal method is required to process. Range analysis is that when considering one factor, it is considered that the influence of other factors on the result is balanced, so that it is believed that the difference in the levels of the factor is caused by itself. In the calculation of the range analysis, the average value k_{ZN} and the influence degree T_Z are shown

$$k_{ZN} = \frac{1}{m} \sum_{i=1}^n y_{Zi}, \quad (9)$$

$$T_Z = R_{\max Z} - R_{\min Z}, \quad (10)$$

where i is the test number; Z represents the factor; y is the test result, which is the signal intensity; $n = 32$; $m = 8$; N is the level number. $R_{\max Z} = \max\{k_{Z1}, k_{Z2}, k_{Z3}, k_{Z4}\}$, $R_{\min Z} = \min\{k_{Z1}, k_{Z2}, k_{Z3}, k_{Z4}\}$. In the range analysis, the average value k_{ZN} when $N = 1, 2, 3, 4$ describes the effect of the factor Z on the test result M . Moreover, the influence degree T_Z represents how large the impact of factor Z is. Using the analysis method above, the range analysis result with different k_{ZN} and T_Z are shown in Table IV.

It is observed in Table IV that the range analysis is implemented at different factors and levels. To make the comparative analysis more intuitive, Fig. 3 shows the analysis results represented by a histogram and a line graph. The bar height represents the average of each factor at each level, and the line graph represents the value of the influence degree for different factors.

Fig. 3 shows that the signal intensity M increases with the number of magnets in a row m , though it is not strictly monotonically increasing. This is because an increase in m causes an increase in the radiation source of the SH guided waves, thereby achieving a superposition of a larger number of waves at the focal point, and thus the signal intensity is increased. Moreover, the increase in FPPM remanence magnetization Br cannot always have a positive effect on the signal intensity M , where M reaches a maximum value at 1.0 T. That is to say, simply increasing the bias magnetic field does not always increase M for a PFSH-EMAT. In addition, the coil width w shows a very good relationship with M , and a higher value of w will lead to a larger M .

As for the coil winding number n , it is undoubtedly that the more coil winding will lead to a larger signal. However, the aperture angle θ shows a nonlinear relationship with M , and EMATs with 20° and 80° angle has a higher signal intensity. For the focal length l_F , we can see that M approximately decreases as l_F increases, it can be explained that the intensity of the ultrasonic waves attenuates as the propagation distance increases.

The lift-off distance h_l shows a clear trend, which was studied and proved before [36]. This phenomenon shows that the h_l of the transducer has a close relationship with transmitting and receiving ultrasonic signals, then the increase of h_l will

reduce the signal intensity M in the result analysis. Moreover, the frequency f_c of the excitation current can reduce M when f_c increases, while there is a peak at 600 kHz. This is because an increase in frequency will lead to a reduction in the size of a single radiation source (half wavelength in length), so the effective vibration source size will decrease, thereby reducing the energy of the radiated wave. From another perspective, a decrease in frequency will lead to an increase in the focal area, thereby dispersing energy, which is why there is a turning point in frequency 600 kHz. With regard to the current amplitude I_c , it is shown in Fig. 3 that it increases with M obviously, because the larger excitation currents result in larger vibration amplitude and more ultrasonic energy.

As shown in Fig. 3 and Table IV, the top five power orders of impact is $TG(126.2) > TA(72.6) > TH(65.3) \approx TI(65.1) > TC(60.7)$, and the minimum value is the factor $TB(36.2)$. It indicates that the lift-off distance h_l is the most significant factor that affects the signal intensity M , and the decrease in h_l will significantly increase M . Number of magnets in a row m follows h_l as the second impact factor, and then the impact degree of the frequency f_c , excitation current I_c , and coil width w is reduced successively.

IV. OPTIMAL METHOD AND EXPERIMENTS

According to the orthogonal test results, the influence degree of different factors on M can be obtained. Therefore, the optimization of a PFSH-EMAT can be achieved by reasonable selection and combination of nine test factors. As shown in Fig. 3, we can see that $k_{A4} > k_{A2} > k_{A3} > k_{A1}$, $k_{B3} > k_{B2} > k_{B4} > k_{B1}$, $k_{C4} > k_{C3} > k_{C2} > k_{C1}$, $k_{D4} > k_{D3} > k_{D2} > k_{D1}$, $k_{E1} > k_{E4} > k_{E2} > k_{E3}$, $k_{F1} > k_{F2} > k_{F3} > k_{F4}$, $k_{G1} > k_{G2} > k_{G3} > k_{G4}$, $k_{H2} > k_{H1} > k_{H3} > k_{H4}$, $k_{I4} > k_{I2} > k_{I3} > k_{I1}$. The optimal combination of factors is $A_4(m = 10)$, $B_3(Br = 1 \text{ T})$, $C_4(w = 0.8 \text{ mm})$, $D_4(n = 17)$, $E_1(\theta = 20^\circ)$, $F_1(l_F = 50 \text{ mm})$, $G_1(h_l = 0.5 \text{ mm})$, $H_2(f_c = 600 \text{ kHz})$, $I_4(I_c = 200 \text{ A})$. The PFSH-EMAT with this combination of parameters should have the best signal intensity. Of course, more levels will make the optimization result more accurate, but here we only consider the case of four levels in this work.

To verify the focusing performance of the optimized EMAT, we analyzed it from both simulations and experiments. Fig. 4 shows the experiment setup that can measure the displacement on the plate surface. As the most important source of the signal generation in EMAT, the signal should be modulated and amplified before being processed. Therefore, RPR-4000 PULSER/RECEIVER is selected in the experiment. The FPPM is of Nd-Fe-B magnet, which magnet length, number, and size is the same as that utilized in the simulation. The material of the specimen is aluminum and the coils are excited by a burst current with an amplitude of 200 A, frequency of 600 kHz and bandwidth factor of 5×10^{11} , which can be controlled by the RPR-4000 power using the programming method, and the waveform of the output current can be also monitored. The focal point and structures of the transmitter and the receiver are

TABLE IV
RANGE ANALYSIS OF THE ORTHOGONAL TTEST RESULTS

Results	Level	Factors								
		A	B	C	D	E	F	G	H	I
		m	B_r	w	n	θ	l_E	h_l	f_c	I_c
M (10^{-7} mm)	1	11.878	24.868	13,331	23.543	67.389	66.994	131.039	44.715	14.603
	2	59.168	48.6855	37.472	39.820	33.471	4.661	41.906	88.653	50.653
	3	57.651	58.609	68.406	64.895	26.684	36.463	15.386	36.458	48.273
	4	84.522	61.057	74.0107	64.9618	65.676	19.29	4.889	23.393	79.6908
	Tz	72.6	36.2	60.7	41.4	40.7	47.7	126.2	65.3	65.1

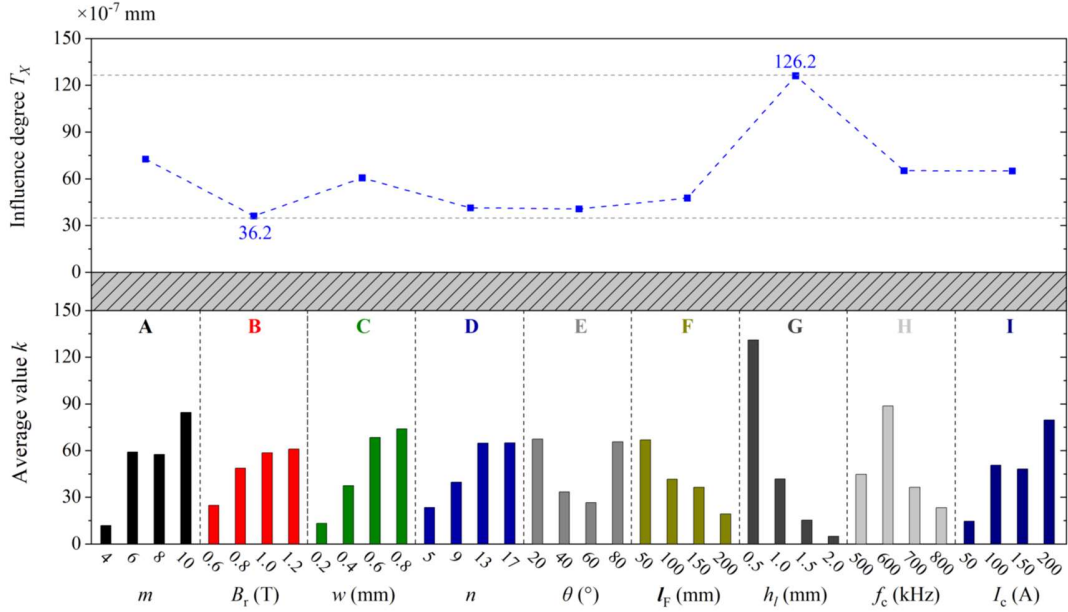


Fig. 3 Range analysis for different factors at different levels. The bar height represents the average of each factor at each level, and the line graph represents the value of the influence degree for different factors. The lift-off distance of the coil has the greatest influence on signal intensity, followed by the number of magnets in a row.

the same. Due to the low energy conversion efficiency of an EMAT, high-power pulse current excitation is required. Therefore, the matching impedances (impedance matching transformers) are utilized in the experiment to achieve the maximum output power of the excitation source.

As a dimensionless processing method that makes the absolute value of a physical system a relative value, the normalization method is used in this work to achieve easy comparison and avoid errors caused by the signal conversion. The normalized standard is the maximum value of the measured signal. Fig. 5 shows the normalized simulation and experimental signal, it can be seen that they are in a good agreement, though there are noise effects in the experiment that will bias the DC component of the signal.

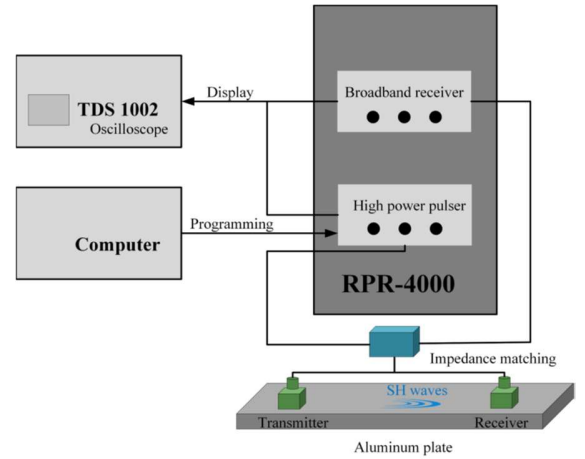


Fig. 4 Experimental configuration of a PFSH-EMAT to optimize the focusing capability

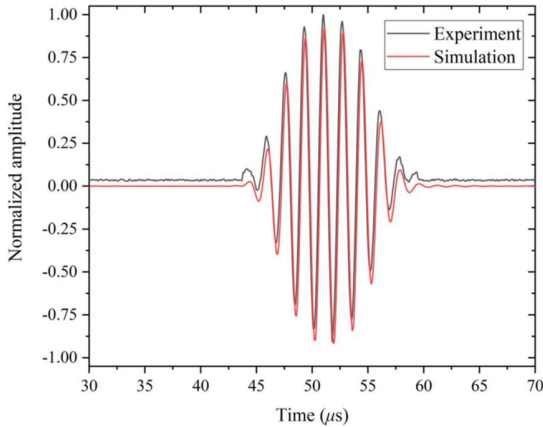


Fig. 5. Simulation and experimental results under the optimized conditions.

To verify the effectiveness of the optimization factor combination, test No. 7, 16 and 30 are selected (the top three signal intensities in the orthogonal test), together with the optimized test in the experiment to measure the signal intensity. Fig. 6 shows the normalized received signal for these four tests. It can be found that the PFSH-EMAT with optimized parameters has a significant advantage over the three non-optimized transducers. The normalized experimental results of test 7, 16, 30 are 0.42, 0.19, and 0.49, respectively. The experimental results show that the signal intensity of the optimized EMAT is 170% higher than that of the average of the top three M in the orthogonal test. It should be emphasized that the selection of more levels in orthogonal experiments will improve the accuracy of PFSH-EMAT optimization, but the method is consistent with this paper.

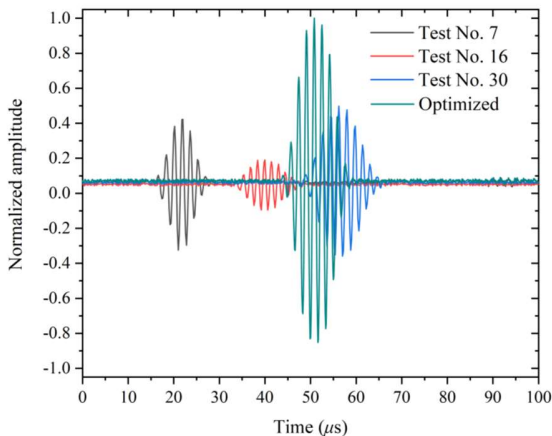


Fig. 6. Experimental results of the received signal for test No. 7, 16, 30 and optimized parameters.

V. CONCLUSIONS

In this work, the impact factors of a PFSH-EMAT are investigated using an L32(49) orthogonal table. Finite element simulations are performed for different combinations of factors to obtain the signal intensity, which is selected as the orthogonal test result. Range analysis of the test results shows that the top

five power orders of impact are $T_G (126.2) > T_A(72.6) > T_H(65.3) \approx T_I (65.1) > T_C(60.7)$, and the minimum value is the factor TB(36.2). This indicates that the lift-off distance of the coil has the greatest influence on the signal intensity, followed by the number of magnets in a row as the second impact factor. Moreover, the relationship between the trend of each factor and the signal intensity is also obtained. By extracting the maximum value of each factor, the optimal combination of parameters can be obtained, so the maximum value of the transducer focusing intensity can be achieved. The experimental results show that the signal intensity of the optimized EMAT is 170% higher than that of the average of the top three signal intensities in the orthogonal test, which proves the effectiveness of the orthogonal test optimization method in this paper.

REFERENCES

- [1] M. Hirao and H. Ogi, "An SH-wave EMAT technique for gas pipeline inspection," *NDT & E Int.*, vol. 32, no. 3, pp. 127–132, Apr. 1999.
- [2] C. B. Thring, Y. Fan, and R. S. Edwards, "Multi-coil focused EMAT for characterisation of surface-breaking defects of arbitrary orientation," *NDT & E Int.*, vol. 88, pp. 1–7, Jun. 2017.
- [3] S. Wang, S. Huang, Y. Zhang, and W. Zhao, "Multiphysics modeling of a Lorentz force-based meander coil electromagnetic acoustic transducer via steady-state and transient analyses," *IEEE Sensors J.*, vol. 16, no. 17, pp. 6641–6651, Sep. 2016.
- [4] S. Legendre, D. Massicotte, J. Goyette, and T. K. Bose, "Neural classification of Lamb wave ultrasonic weld testing signals using wavelet coefficients," *IEEE Trans. Instrum. Meas.*, vol. 50, no. 3, pp. 672–678, Jun. 2001.
- [5] S. Legendre, D. Massicotte, J. Goyette, and T. K. Bose, "Wavelettransform- based method of analysis for Lamb-wave ultrasonic NDE signals," *IEEE Trans. Instrum. Meas.*, vol. 49, no. 3, pp. 524–530, Jun. 2000.
- [6] J. J. da Silva, M. G. Wanzeller, P. de Almeida Farias, and J. S. da Rocha Neto, "Development of circuits for excitation and reception in ultrasonic transducers for generation of guided waves in hollow cylinders for fouling detection," *IEEE Trans. Instrum. Meas.*, vol. 57, no. 6, pp. 1149–1153, Jun. 2008.
- [7] S. Huang, L. Peng, Q. Wang, S. Wang, and W. Zhao, "An opening profile recognition method for magnetic flux leakage signals of defect," *IEEE Trans. Instrum. Meas.*, vol. 68, no. 6, pp. 2229–2236, Jun. 2019.
- [8] D. I. Ona, G. Y. Tian, R. Sutthaweekul, and S. M. Naqvi, "Design and optimisation of mutual inductance based pulsed eddy current probe," *Measurement*, vol. 144, pp. 402–409, Oct. 2019.
- [9] H. M. Seung, C. I. Park, and Y. Y. Kim, "An omnidirectional shearhorizontal guided wave EMAT for a metallic plate," *Ultrasonics*, vol. 69, pp. 58–66, Jul. 2016.
- [10] N. Nakamura, H. Ogi, and M. Hirao, "Detection of shear horizontal guided waves propagating in aluminum plate with thinning region," *Jpn. J. Appl. Phys.*, vol. 50, no. 7S, Dec. 2013, Art. no. 07HC17.

- [11] Y. Zhang, S. Huang, S. Wang, and W. Zhao, "Direction-controllable electromagnetic acoustic transducer for sh waves in steel plate based on magnetostriction," *Prog. Electromagn. Res. M*, vol. 50, pp. 151–160, Jan. 2016.
- [12] G. Waag, L. Hoff, and P. Norli, "Air-coupled ultrasonic throughtransmission thickness measurements of steel plates," *Ultrasonics*, vol. 56, pp. 332–339, Feb. 2015.
- [13] X. Wang *et al.*, "An air-coupled capacitive micromachined ultrasound transducer for noncontact nondestructive evaluation," in *Proc. IEEE Sensors*, Oct. 2007, pp. 1464–1467.
- [14] R. Ribichini, F. Cegla, P. Nagy, and P. Cawley, "Study and comparison of different EMAT configurations for SH wave inspection," *IEEE Trans. Ultrason., Ferroelectr., Freq. Control*, vol. 58, no. 12, pp. 2571–2581, Dec. 2011.
- [15] N. Lunn, S. Dixon, and M. D. G. Potter, "High temperature EMAT design for scanning or fixed point operation on magnetite coated steel," *NDT & E Int.*, vol. 89, pp. 74–80, Jul. 2017.
- [16] H. Ogi, M. Hirao, and T. Ohtani, "Line-focusing of ultrasonic SV wave by electromagnetic acoustic transducer," *J. Acoust. Soc. Amer.*, vol. 103, no. 5, pp. 2411–2415, May 1998.
- [17] H. Ogi, M. Hirao, and T. Ohtani, "Line-focusing electromagnetic acoustic transducers for the detection of slit defects," *IEEE Trans. Ultrason., Ferroelectr., Freq. Control*, vol. 46, no. 2, pp. 341–346, Mar. 1999.
- [18] N. Nakamura, K. Ashida, T. Takishita, H. Ogi, and M. Hirao, "Inspection of stress corrosion cracking in welded stainless steel pipe using point-focusing electromagnetic-acoustic transducer," *NDT & E Int.*, vol. 83, pp. 88–93, Oct. 2016.
- [19] X. Zhao and J. L. Rose, "Guided circumferential shear horizontal waves in an isotropic hollow cylinder," *J. Acoust. Soc. Amer.*, vol. 115, no. 5, pp. 1912–1916, May 2004.
- [20] J. K. Lee, H. W. Kim, and Y. Y. Kim, "Omnidirectional Lamb waves by axisymmetrically configured magnetostrictive patch transducer," *IEEE Trans. Ultrason., Ferroelectr., Freq. Control*, vol. 60, no. 9, pp. 1928–1934, Sep. 2013.
- [21] X. Song and G. Qiu, "Optimization of a focusable and rotatable shearwave periodic permanent magnet electromagnetic acoustic transducers for plates inspection," *Sensors*, vol. 17, no. 12, p. 2722, Nov. 2017.
- [22] H. Sun, S. Wang, S. Huang, Q. Wang, and W. Zhao, "Point-focusing of shear-horizontal wave using fan-shaped periodic permanent magnet focusing coils EMAT for plate inspection," *IEEE Sensors J.*, vol. 19, no. 12, pp. 4393–4404, Jun. 2019.
- [23] H. Sun, S. Huang, Q. Wang, S. Wang, and W. Zhao, "Improvement of unidirectional focusing periodic permanent magnet shear-horizontal wave electromagnetic acoustic transducer by oblique bias magnetic field," *Sens. Actuators A, Phys.*, vol. 290, pp. 36–47, May 2019.
- [24] S. L. Huang, H. Y. Sun, Q. Wang, S. Wang, and W. Zhao, "Unidirectional focusing of horizontally polarized shear elastic waves electromagnetic acoustic transducers for plate inspection," *J. Appl. Phys.*, vol. 125, no. 16, Apr. 2019, Art. no. 164504.
- [25] Z. Liu, L. Deng, Y. Zhang, A. Li, W. Bin, and C. He, "Development of an omni-directional magnetic-concentrator-type electromagnetic acoustic transducer," *NDT & E Int.*, vol. 109, Jan. 2020, Art. no. 102193.
- [26] L. Kang, S. Dixon, K. Wang, and J. Dai, "Enhancement of signal amplitude of surface wave EMATs based on 3-D simulation analysis and orthogonal test method," *NDT & E Int.*, vol. 59, pp. 11–17, Oct. 2013.
- [27] L. Kang, C. Zhang, S. Dixon, H. Zhao, S. Hill, and M. Liu, "Enhancement of ultrasonic signal using a new design of Rayleigh-wave electromagnetic acoustic transducer," *NDT & E Int.*, vol. 86, pp. 36–43, Mar. 2017.
- [28] C. B. Thring, Y. Fan, and R. S. Edwards, "Focused Rayleigh wave EMAT for characterisation of surface-breaking defects," *NDT & E Int.*, vol. 81, pp. 20–27, Jul. 2016.
- [29] X. Jian, S. Dixon, K. T. V. Grattan, and R. S. Edwards, "A model for pulsed Rayleigh wave and optimal EMAT design," *Sens. Actuators A, Phys.*, vol. 128, no. 2, pp. 296–304, Apr. 2006.
- [30] T. Takishita, K. Ashida, N. Nakamura, H. Ogi, and M. Hirao, "Development of shear-vertical-wave point-focusing electromagnetic acoustic transducer," *Jpn. J. Appl. Phys.*, vol. 54, no. 7S1, Jun. 2015, Art. no. 07HC04.
- [31] X. Jia and Q. Ouyang, "Optimal design of point-focusing shear vertical wave electromagnetic ultrasonic transducers based on orthogonal test method," *IEEE Sensors J.*, vol. 18, no. 19, pp. 8064–8073, Oct. 2018.
- [32] J. Peng *et al.*, "Orthogonal test design for optimization of supercritical fluid extraction of daphnoretin, 7-methoxy-daphnoretin and 1,5- diphenyl-1-pentanone from *stellera chamaejasme* L. And subsequent isolation by high-speed counter-current chromatography," *J. Chromatogr. A*, vol. 1135, no. 2, pp. 151–157, Dec. 2006.
- [33] D. MacLauchlan *et al.*, "Recent advancements in the application of Emats to NDE," in *Proc. 16th WCNDT*, Montreal, QC, Canada, 2004, pp. 1154–1161.
- [34] X. Jian, S. Dixon, R. S. Edwards, and J. Morrison, "Coupling mechanism of an EMAT," *Ultrasonics*, vol. 44, pp. e653–e656, Dec. 2006.
- [35] S. Huang, H. Sun, S. Wang, Q. Wang, and W. Zhao, "Numerical evaluation of focal position selection by line-focusing electromagnetic acoustic transducer with experimental validation," *Int. J. Appl. Electromagn. Mech.*, vol. 61, no. 3, pp. 341–355, Nov. 2019.
- [36] S. Huang, W. Zhao, Y. Zhang, and S. Wang, "Study on the lift-off effect of EMAT," *Sens. Actuators A, Phys.*, vol. 153, no. 2, pp. 218–221, Aug. 2009.



Hongyu Sun received the B.S. degree from the Department of Renewable Energy, and the master's degree from the Department of Electrical and Electronic Engineering, North China Electric Power University, Beijing, China, in 2018 and 2015, respectively. He is currently pursuing the Ph.D. degree with the Department of Electrical Engineering, Tsinghua University. His major research interests include electromagnetic measurement, nondestructive evaluation, acoustic metamaterials, and plasma physics.



Qing Wang (Senior Member, IEEE) received the B.Eng. degree in electronic instrument and measurement technique from Beihang University, Beijing, China, in 1995, the M.Sc. degree in advanced manufacturing and materials from the University of Hull, Hull, U.K., in 1998, and the Ph.D. degree in manufacturing management from De Montfort University, Leicester, U.K., in 2001. She is currently an Associate Professor with the School of Engineering and Computing Sciences, Durham University, Durham, U.K. Her research interests include electronic instruments and measurement, computer simulation, and advanced manufacturing technology.



Shen Wang received the bachelor's and Ph.D. degrees in electrical engineering from Tsinghua University, Beijing, China, in 2002 and 2008, respectively. He is currently a Research Assistant with the Department of Electrical Engineering, Tsinghua University. His research interests include nondestructive testing and evaluation, and virtual instrumentation.



Wei Zhao received the bachelor's degree in electrical engineering from Tsinghua University, Beijing, China, in 1982, and the Ph.D. degree from the Moscow Power Engineering Institute Technical University, Moscow, Russia, in 1991. He is currently a Professor with the Department of Electrical Engineering, Tsinghua University. His research interests include modern electromagnetic measurement and instrument techniques.



Songling Huang (Senior Member, IEEE) received the bachelor's degree in automatic control engineering from Southeast University, Nanjing, China, in 1991, and the Ph.D. degree in nuclear application technology from Tsinghua University, Beijing, China, in 2001. He is currently a Professor with the Department of Electrical Engineering, Tsinghua University. His research interests include non-destructive evaluation and instrument techniques.



Jun Zou received the bachelor's degree in power system and automation from the Zhengzhou Institute of Technology, China, in 1994, the master's degree in power system and automation from the Zhengzhou University of Technology, China, in 1997, and the Ph.D. degree in electrical engineering from Tsinghua University, Beijing, China, in 2001. He is currently a Professor with the Department of Electrical Engineering, Tsinghua University. His research interests include electromagnetic environment and grounding technology, electromagnetic pulse transient analysis, electromagnetic field numerical calculation.



Lisha Peng (Student Member, IEEE) received the bachelor's degree from Wuhan University, Hubei, China, in 2014, and the Ph.D. degree from the Department of Electrical Engineering, Tsinghua University in 2019. She is currently a Postdoctoral with the Department of Electrical Engineering, Tsinghua University. Her current research interests include magnetic flux leakage (MFL) measurement and defect estimation.